

## Evaluation of neck lesions with MDCT – A case series

Dr. Dhaval K Thakkar<sup>1</sup>, Dr. Sanjay Khaladkar<sup>2</sup>, Dr. Mansi Jantre<sup>3</sup>,  
Dr. Dolly K Thakkar<sup>4</sup>, Dr. Amarjit Singh<sup>5</sup>, Dr. Vilas M. Kulkarni<sup>6</sup>.

1-Chief Resident, Dept. of Radiodiagnosis, Dr D Y Patil Medical college and Research centre, Pimpri, Maharashtra, India; 2-Professor, Dept. of Radiodiagnosis, Dr D Y Patil Medical college and Research centre, Pimpri, Maharashtra, India; 3-Senior Resident, Dept. of Radiodiagnosis, Dr. D Y Patil Medical college and Research centre, Pimpri, Maharashtra, India; 4- Senior Resident, KEM hospital, Mumbai, Maharashtra, India; 5- Dean & Professor, Dept. of Radiodiagnosis, Dr. D Y Patil Medical college and Research centre, Pimpri, Maharashtra, India; 6-Professor, Dept. of Radiodiagnosis, Dr D Y Patil Medical college and Research centre, Pimpri, Maharashtra, India.

### Abstract:

**Aim** Our study aimed at evaluating the role of MDCT for the detection and characterization of various neck lesions and characterization of lymph nodes as benign or malignant. **Material and methods-** This study was carried out in 100 patients of neck lesions suspected clinically or by previously performed ultrasonography in the Department of Radio-diagnosis, Dr. D. Y. Patil Medical College and Research Centre, Pimpri, Pune after approval from the ethics committee on 'Philips Ingenuity 128 Slice CT Scanner. The CT findings of neck lesions were analyzed on plain and contrast study. **Results.** There was male preponderance (66%), with females accounting for 34% of total cases. 34/100 (34%) were of malignant etiology, 24 (24%) were of benign etiology, 33(33%) inflammatory etiology, 6(6%) were congenital and 3(3%) were of vascular etiology. The main differentiating features between benign and malignant lesions were well-defined margins and fat plane for benign lesions. Cystic hygroma (3/6=50%) was most common congenital lesions, IJV thrombosis (2/3=66.67%) in vascular lesions, retropharyngeal abscess (6/33=18.18%) in inflammatory lesions. Goiter (5/24=20.83%) predominated followed by parathyroid adenoma (4/24=16.67%) in benign lesions. In malignant etiology, metastatic lymph nodes were seen in (7/34=20.58%), primary malignancy could be detected in 24/34 (70.58%) cases. Visceral space (31%) was the most commonly involved neck space. The CT imaging diagnosis was confirmed with biopsy, FNAC, surgery, or by pathognomic imaging findings on contrast enhanced CT. **Conclusion** MDCT proved to be a very useful non- invasive tool in accurately diagnosing and characterizing neck lesions.

**Keywords:** CT Neck, Neck spaces, cervical lymphadenopathy, benign and malignant neck masses

### I. Introduction

A mass lesion in the neck can be a diagnostic challenge in a patient of any age. Neck masses include a spectrum of lesions of diverse origin and etiology. Clinical examination alone is limited in its ability to accurately assess the extent and size of head and neck tumors, especially or submucosal extension of disease and extent of nodal metastasis. <sup>[1]</sup> Computed tomography has found an increasing application in the evaluation of neck masses—both congenital and acquired, and is currently one of the most powerful and versatile imaging procedures for the evaluation of neck masses. <sup>[2]</sup> Multislice spiral CT provides volumetric helical data, thereby permitting optimal multiplanar and 3D reconstructions and isotropic imaging. Rapid scan acquisition reduces motion artifacts, as well as permits phonation studies. Imaging during phonation and/or Valsalva maneuver to assess vocal cords mobility in pathologies involving hypopharynx.

The neck is divided into suprahyoid and infrahyoid parts by the hyoid bone. The suprahyoid neck spaces include pharyngeal mucosal space, parapharyngeal space, masticator space, parotid space, carotid space, retropharyngeal space, submandibular and sublingual space, and perivertebral space. The infrahyoid neck spaces include visceral space, carotid space, retropharyngeal space, perivertebral space, and posterior cervical space.

By allocation of a tumor to a certain space the number of differential diagnosis drops dramatically due to the fact that in different compartments different type soft tissues occur. <sup>[3]</sup> The main goal of head and neck imaging is to evaluate the true extent of disease to best determine surgical and therapeutic options. This process includes evaluation of the size, location, and extent of tumor infiltration into surrounding vascular and visceral structures. Second, nodal staging should be assessed by a standard classification system that can be understood and consistently applied by the radiologist, surgeon and radiation oncologist. CT is fast, well tolerated, readily reformatted into multiple imaging planes, excellent for evaluating bony framework and small calcifications, as

well as readily available but has lower contrast resolution and requires iodinated contrast and ionizing radiations. CT is ideal for initial evaluation, preoperative planning, biopsy targeting, and postoperative follow up.<sup>(1)</sup>

**II. Materials And Methods**

This study was carried out in 100 patients of neck lesions suspected of having neck lesions (suspected clinically or by previously performed ultrasonography) in the Department of Radio-diagnosis, Dr. D. Y. Patil Medical College and Research Centre, Pimpri, Pune after approval from the ethics committee on ‘Philips Ingenuity 128 Slice CT Scanner. Post operative , post radiation therapy, skull base lesions, in whom contrast was contraindicated were excluded. Written informed consent was obtained from each patient or from parents in cases of pediatric patients. Imaging was done during quiet breathing. Puffed cheek technique was used to outline gingivobuccal sulcus in suspected cases of Ca buccal mucosa. Valsalva’s maneuver with phonation was use to distend pyriform sinuses. Region from skull base to clavicles was covered during non contrast and contrast enhanced CTscan. Parameters used were– patient position being ‘head first supine’; scan type was axial/helical; table speed = 81.2 mm/sec; scan length depending on area covered; scan time being 5-6 secs; collimation = 64 x 0.625 mms; slice thickness = 3mms; pitch = 1.026; rotation time = 0.50 secs; field of view = 250-300 mms; voltage = 120 kVs; current = 160-180 mAs; Image matrix = 512 x 512; CT does length volume (CTDLVol) = 5.4 mGys.

The CT findings were analyzed for location, margins of the lesion, density on plain study, enhancement pattern, presence of calcification and necrosis, extension into adjoining structures, presence or absence of vascular and bone involvement and presence or absence of metastasis in malignant lesions.

**III. Observations And Results**

A total of 100 patients underwent CT head and neck examination. The CT imaging diagnosis was confirmed with biopsy, FNAC, surgery, or by pathognomic CECT findings or biochemical correlation. Distribution and observations in these patients are as follows:

	No. of patients	Percentage
<b>Males</b>	66	66%
<b>Females</b>	34	34%
<b>Total</b>	100	100%

**Table 1:** Sex distribution of cases.

**Table - 2:** Distribution of various pathologies in neck spaces:

Sr. No.	Pathology	Total no. of patients	Percentage (%)
1	Malignant	34	34
2	Benign	24	24
3	Inflammatory	33	33
4	Congenital	06	06
5	Vascular	03	03
	<b>Total</b>	100	100

Majority of the pathologies were malignant (34%), followed by inflammatory (33%). Benign lesions accounted for 24%, congenital for 6% and vascular for 3%.

**Table no. 3-** Analysis of various neck conditions based on their etiology with their respective anatomic neck space distribution.

Sr. No.	Conditions	Total	Neck space
<b>1.</b>	<b>Congenital</b>	6	
	• Thyroglossal cyst	2	VS
	• Cystic hygroma	3	PCS
	• Ranula	1	SLS
<b>2.</b>	<b>Vascular</b>	3	
	• IJV thrombosis	2	CS
	• ICA aneurysm	1	CS

4.	<b>Inflammatory</b>	33		
	• Thyroiditis	1	VS	
	• Adenoid hypertrophy	5	PMS	
	• Parotitis	4	PS	
	• Parotid abscess	3	PS	
	• Tuberculous lymphadenitis	3	CS	
	• Post dental infection	2	MS	
	• Retropharyngeal abscess	6	RPS	
	• Peritonsillar abscess	1	PMS	
	• Tonsillitis	1	PMS	
	• Parapharyngeal space abscess	1	PPS	
	• Chronic sialoadenitis with atrophy	1	SMS	
	• Tuberculous cervical spine	3	PVS	
	• Left submandibular abscess	2	SMS	
	5.	<b>Benign</b>	24	
		• Parathyroid adenoma	4	VS
		• Goitre	5	VS
		• Colloid cyst	1	VS
		• Angiofibroma	2	PMS
		• Schwannoma	1	CS
• Paraganglioma		1	CS	
• Multinodular goiter		1	VS	
• Warthin's tumour		2	PS	
• Pleomorphic adenoma		1	PS	
• Retention cyst (parotid)		2	PS	
• Recurrent adamantinoma		1	MS	
• Ivory osteoma		2	MS	
• Parotid duct stricture	1	PS		
5.	<b>Malignant</b>	34		
	• Metastatic lymph nodes	7	CS	
	• Primary lymphoma	3	PMS+PCS	
	• Primary malignancy	24		
	• Supra-glottic Ca	7	VS	
	• Infra-glottic Ca	1	VS	
	• Thyroid malignancy	7	VS	
	• Ca Cervical oesophagus	2	VS	
	• Ca Alveolus	1	MS	
	• Ca soft palate	1	PMS	
	• Ca buccal mucosa	3	BS	
• Ca oropharynx	2	BS		

Cystic hygroma (3/6=50%) was the most common of all congenital lesions. IJV thrombosis (2/3=66.67%) predominated vascular lesions, retropharyngeal abscess (6/33=18.18%) predominated in inflammatory lesions. Of all benign lesions, goiter (5/24=20.83%) predominated followed by parathyroid adenoma (4/24=16.67%). In malignant etiology, predominate lesions were of nodal metastasis, supra-glottic Ca and thyroid malignancy (7/34=20.58% each).

**Table– 4:** Distribution of pathologies in the various neck spaces.

Sr. No.	Pathology	Total no. of patients	Percentage (%)
1	Parapharyngeal space	1	1%
2	Pharyngeal mucosal space	13	13%
3	Carotid space	12	12%
4	Parotid space	12	12%
5	Masticator space	7	7%
6	Retropharyngeal space	6	6%
7	Posterior cervical space	6	6%
8	Perivertebral space	4	4%
9	Submandibular space	3	3%
10	Sublingual space	1	1%
11	Visceral space	31	31%
12	Buccal space	4	4%

Maximum number of lesions were recorded in the visceral space (31%) followed by those in the pharyngeal mucosal space (13%) and carotid and parotid space (12% each). While minimum number of lesions were recorded in parapharyngeal space and sublingual space.

**Table– 5:** Age distribution of malignant, benign, inflammatory, congenital and vascular lesions.

Age	Benign	Malignant	Inflammatory	Congenital	Vascular	Total
1-20	3	0	8	0	0	11
21-40	5	1	6	4	0	16
41-60	3	15	13	0	3	34
61-80	12	14	5	2	0	33
>81	1	4	1	0	0	6

Majority of patients were in the age group of 41 to 60 years (n= 34), followed by 61 to 80 years (n= 33) and 21 to 40 years (n = 16). 97% of malignant lesions were above 40 years of age. 67% of non malignant lesions were below the age of 60 years. Benign lesions were seen maximum (50%) in the age group of 61-80 years, inflammatory (39.39%) in 41-60 years, congenital (66.67%) in 21-40 years and vascular (100%) in 41-60 years of age group.

**Table– 6:** Distribution of etiologies in various neck spaces.

Sr. No.	Neck Spaces	Benign	Malignant	Inflammatory	Congenital	Vascular	Total
1	PPS	-	-	1	-	-	1
2	PMS	2	4	7	-	-	13
3	CS	2	5	2	-	3	12
4	PS	5	-	7	-	-	12
5	MS	4	1	2	-	-	7
6	RPS	-	-	6	-	-	6
7	PCS	-	2	1	3	-	6
8	PVS	-	1	3	-	-	4
9	SMS	-	-	3	-	-	3
10	SLS	-	-	-	1	-	1
11	VS	11	17	1	2	-	31
12	BS	-	4	-	-	-	4

Of the lesions involving the suprahyoid neck spaces, the maximum number of lesions were recorded in the pharyngeal mucosal space (n=13) followed by the carotid and parotid space each (n=12).

In the Pharyngeal mucosal space (n=13) majority of lesions were of inflammatory origin, 7 out of 13 (53.84 %). In the carotid space (n=12) majority of lesions were of malignant etiology, 5 out of 12 (41.66%), while in the parotid space (n=12) majority of the lesions were of inflammatory origin, 7 out of 12 (58.33%).Of the lesions involving the infrahyoid neck, the predominant lesions were observed in the visceral space (n=31), of which majority of lesions were of malignant etiology, 17 out of 31 (54.83%).

The CT findings were analyzed for location, margins of the lesion, density on plain study, enhancement pattern, presence of calcification and necrosis, extension into adjoining structures, presence or absence of vascular and bone involvement and presence or absence of metastasis in malignant lesions.

**Table 7-** CT characteristics of benign, malignant and inflammatory, congenital and vascular lesions.

SN	CT Findings	Benign (24)	Malignant (34)	Inflammation (33)	Congenital (6)	Vascular (3)
1.	<b>Margins</b>					
	• Well defined	23	07	21	6	3
	• Ill defined	1	27	12	-	-
2.	<b>Density (on plain scan)</b>					
	• Hypodense	2	10	13	-	-
	• Isodense	-	-	-	-	1
	• Hyperdense	2	-	-	-	-
	• Heterogeneous	16	24	20	-	2
	• Cystic	4	-	-	6	-
3.	<b>Enhancement (post contrast)</b>					
	• Homogeneous					
	• Intense	-	-	-	-	1
	• Moderate	4	4	9	-	-
	• Mild	-	-	-	-	-
	• Heterogeneous	14	30	11	-	-
	• Non-enhancing	6	-	-	6	2
	• Central Hypodense with peripheral enhancement	-	-	13	-	-
4.	<b>Necrosis</b>	14	30	11	-	-

5.	Calcification	3	-	-	-	-
6.	Extension into adjacent spaces	02	20	05	2	-
7.	Vascular involvement	-	07	02	-	3
8.	Obliteration of intermuscular fat planes	2	27	9	2	-
9.	Air pockets	-	-	02	-	-
10.	Bone involvement	04	07	08	-	-

#### IV. Discussion

CT scans of 100 patients who were found to have lesions of neck were characterized and analyzed.

Out of the 100 cases studied, 34(34%) were of malignant etiology, 24 (24%)were of benign etiology, 33(33%) were of inflammatory etiology, 6(6%) were congenital and 3(3%) were of vascular etiology. The main differentiating features between benign and malignant lesions were well-defined margins and fat plane for benign lesions. Inflammatory lesions demonstrated mild to moderate fat plane obliteration, thick peripheral rim enhancement and presence of air pockets. While malignant lesions revealed ill-defined margins, loss of fat plane, heterogeneous enhancement, extension beyond fascial planes,vascular and bone involvement as well as metastasis to lymph nodes.

In our study, 45 out of 66 (68.18%) benign lesions of the head and neck region including the inflammatory, congenital and vascular causes were below the age of 60 years. Whereas, 33 out of 34 (97.05%) of the malignant lesions of the head and neck region in this series were above the age of 40 years except for 1 case wherein a case of B cell lymphoma in pharyngeal mucosal space was diagnosed in a 40 years old male. A study done by Ozkiris M et al also showed that in neck masses, neoplasms should be considered in older adults and inflammatory and congenital masses in children and young patients.<sup>[4]</sup>

In the present study male predominance of malignant lesions were detected with a male to female ratio of 1.8:1. Most of the malignant lesions of the neck were found among the males. This could be attributed to the smoking and alcohol habits. A study done by Abhinandan Bhattajaree et al. showed a male preponderance of malignant lesions in neck.<sup>[5]</sup>

The most common primary malignant lesion in the neck in the present study was carcinoma of pyriform fossa (hypopharynx) 6 out of 34 cases (17.64%) and thyroid carcinoma 5 out of 34 cases (14.70%). In a study by Savita Lasrado et al the most common site of primary malignant lesion in the neck was larynx(19.6%), followed by the thyroid(14.4%), the tongue and hypopharynx with 10.3%cases each.<sup>[6]</sup> The most common space involved in the present study was visceral space (31%) followed by pharyngeal mucosal space (13%) due to higher incidence of pyriform fossa and thyroid carcinomas. This corresponds to the study performed by Shreshtha MK et al in which, maximum number of lesions in the suprahyoid neck were in the pharyngeal mucosal space (n=21) and in the infrahyoid neck maximum cases (40) were confined to the visceral space.<sup>[7]</sup>

7 out of 100 cases were localized to have masticator space involvement. 4 were benign lesions(e.g. adamantinoma, osteoma, stricture in distal Stensons duct causing cystic dilatation of duct adjacent to masseter muscle), 1 malignant lesion (carcinoma alveolus) and 2 inflammatory lesions (post dental extraction osteomyelitis of mandible).

A study done by Galli F et al concluded that computed tomography was effective in the identification of the origin of non-extensive lesions involving masticator space and should be chosen in cases with suspected inflammatory involvement of mandible bone.<sup>[8]</sup>

4 out of 100 cases of buccal space lesions were encountered. All were malignant involving the buccal mucosa with extension to involve the buccal space. CT accurately diagnosed all cases. Malignant lesions were characterized by ill-defined margins, loss of fat plane with adjacent structures, violation of fascial planes, aggressive bone destruction and metastasis to lymph nodes. In addition, puffed-cheek CT scans provided a clearer and more detailed evaluation of mucosal surfaces than conventional scans. Yasuokimura et al concluded that buccal space was the most common site of spread from upper and lower gingival cancers, followed by masticator space. Therefore, buccal space should be monitored carefully for possible cancer extension, because involvement of the posterior part of the buccal space may lead to a further extension of the cancer into the masticator space and then into the skull base.<sup>[9]</sup>

12 out of 100 cases of parotid lesions were encountered out of which 5 cases were of benign etiology (e.g. pleomorphic adenoma, Warthins tumor, retention cyst) and 7 cases of inflammatory origin (4 cases of parotitis and 3 cases of parotid abscess). The benign tumors revealed well-defined margins, homogenous enhancement, and were located in the superficial lobe.

In the 4 cases of parotitis, CT could identify an obstructing calculus in the distal duct in 3 cases, and enlarged homogeneously enhancing parotid gland. Parotid abscesses revealed thick peripheral enhancement with central necrosis/ liquefaction.

Shin K. H conducted a study of parotid gland tumors and used criteria of location, size, density, margin, calcification within tumors, necrosis, cystic change, invasion of extra glandular structure and lymphadenopathy. Irregularities in tumor margin and findings of extra glandular extension are the most helpful indicators by which benign and malignant parotid tumors may be differentiated.<sup>[10]</sup>

13 out of 100 cases of pharyngeal mucosal space lesions were diagnosed (e.g. adenoidal hypertrophy (n=5), oropharyngeal carcinoma (n=3), juvenile nasopharyngeal angiofibroma (n=2) and a case each of peritonsillar abscess, tonsillitis and lymphoma.

Nasopharyngeal angiofibroma characteristically involved the pterygopalatine fissure, nasopharynx with secondary invasion of the maxillary and ethmoid sinuses. Both cases showed intracranial extension and characteristic intense vascular enhancement on post contrast administration. This is comparable with study conducted by Bhaskar Ghosh et al.<sup>[11]</sup>

6 out of 100 cases of retropharyngeal abscesses were diagnosed. 2 cases were associated with erosion of the vertebral body and 4 cases showed extension into surrounding visceral and carotid spaces. This is consistent with the findings of Federici S et al who concluded that the accuracy of CT was 71.4% in correctly identifying an abscess, and that CT scan is indicated to assess the extent of infection and exclude complications.<sup>[12]</sup>

6 out of 100 lesions were detected in the posterior cervical space. Three cases each of lymph nodes and cystic hygroma were detected. 2 Out of the 3 cases of lymphadenopathy were due to lymphoma. CT showed multiple, bilateral, non-necrotic and homogeneously enhancing lymph node involvement. Tuberculous lymphadenitis was diagnosed by identifying peripheral enhancement and central non enhancing necrosis associated with cold abscess tracking along the fascial plane on CT, which was later confirmed on culture examinations of the tissue sample.

This is comparable with a study by Geoffrey D parker et al, they showed that most common lesion in the PCS involved the lymph nodes, i.e metastatic lymph nodes followed by lymphomatous lymph nodes.<sup>[13]</sup>

31/100 cases were encountered in the visceral space. The pathologies found were hypopharyngeal carcinomas (n=8), carcinoma of thyroid gland (n=7), goiter (n=6), parathyroid adenomas (n=4), thyroglossal cyst (n=2), and each case of carcinoma epiglottitis, thyroiditis, colloid cyst and carcinoma of esophagus.

The parathyroid adenomas were identified by their characteristic arterial hyper- enhancement and location. This is consistent with a study done by Geneva J Randall et al.<sup>[14]</sup>

6 cases were of congenital origin - thyroglossal cyst in the visceral space was the most common congenital lesion (n=2) This is comparable with the study performed by Al-Khateeb TH et al who concluded that the most frequent congenital neck mass was thyroglossal duct cyst, followed by cysts of the branchial apparatus.<sup>[15]</sup> 12 out of 100 cases of carotid space lesions were diagnosed. Out of these seven were lymph-node masses (e.g. tuberculosis n=2 and metastatic lymph nodes n=5), vascular lesions n=3 (e.g. two IJ.V thrombus and one ICA aneurysm) and a case each of vagal schwannoma and paraganglioma were encountered in the series. The metastatic lymph nodes revealed central necrosis and ill-defined margins with IJV invasion suggestive of extra-capsular spread. The schwannoma was well circumscribed, homogenous enhancement with focal hypodensities within and lateral to carotid sheath.

3 out of 100 cases were encountered in the submandibular space (one case of acute on chronic sialadenitis and two cases of submandibular abscess). CT revealed multiple submandibular gland calculi with atrophy of the gland and a small collection posterior to the large left submandibular calculus indicative of an acute on chronic sialadenitis. The submandibular abscess had low attenuation necrotic, pus filled center and thick irregular enhancing rim with adjacent fat stranding.

4 out of 100 cases were detected in the perivertebral space - 3 cases of Koch's spine and 1 case of vertebral metastasis. CT could identify vertebral body destruction with evidence of prevertebral and paravertebral soft tissue in cases of Koch's spine and revealed posterior spinal element involvement in metastasis from carcinoma prostate.

A total of 33 deep neck space infections (7 each in pharyngeal mucosal space and parotid space, 6 retropharyngeal, 3 each in perivertebral space and submandibular space, 2 each in the carotid and masticator space, 1 each in posterior cervical, visceral and parapharyngeal space) were encountered, which were accurately diagnosed by CT. The most frequently infected neck space was PMS. This correlated with study by Khaled et al (2010) in which most frequently infected neck space was the peritonsillar space (pharyngeal mucosal space), followed by the parapharyngeal space.<sup>[16]</sup>

17 malignant lymph nodes were encountered including 3 primary and 14 metastatic. Based on size criteria and central necrotic area CT correctly differentiated benign and malignant lymph nodes that correlate with study done by R A Zoulman et al. Lymph node central necrosis is a useful indicator of metastatic lymph node extracapsular spread, with a sensitivity of 95 per cent, a specificity of 85 per cent. Lymph node diameter is not a sensitive indicator of extracapsular spread.<sup>[17]</sup> The benign lesions like nasopharyngeal angiofibroma, adamantinoma, osteoma caused bony expansion and remodeling rather than bony destruction and erosion. Whereas, malignant lesions like buccal carcinoma, vertebral metastasis, carcinoma mandible caused bony destruction and erosion. Inflammatory lesions like Koch’s spine and retropharyngeal abscess and osteomyelitis of the jaw caused bone erosions and destruction. Extension into the adjacent space was seen in 20 out of 34 (58.82%) malignant lesions and in 2 benign lesions (i.e., two cases of nasopharyngeal angiofibroma).

**Lymph nodes<sup>[18]</sup>**

Extra-capsular spread of tumor is manifested by capsular enhancement, ill-defined nodal margins, obliterated fat planes surrounding the nodes and edema or thickening in adjacent soft tissues. Shape of lymph node is not reliable in differentiating normal from pathological nodes. Ratio of maximal longitudinal to maximal axial diameter of enlarged nodes calculated by spiral CT may be used to differentiate both malignant and reactive nodes. Nodes which are spherical with ratio < 2 are likely to be malignant and nodes with ratio >=2 are likely to be benign or hyperplastic lymph node. Clusters are defined as multiple (>=3) contiguous ill-defined nodes with in the same level ranging from 8mm-15mm in size. Clusters are seen in inflammation, cancer and lymphoma. Criteria for lymph node enlargement are- retropharyngeal more than 8 mms in maximum diameter, 1.5cms in maximum diameter near angle of mandible, more than 1 cm in maximum diameter elsewhere in neck, ratio of maximal longitudinal nodal length to maximal axial nodal length:, >2 = hyperplastic lymph node and <2 = s/o metastatic lymph node

**CASES**

**PARAPHARYNGEAL SPACE**

**Case 1: Left Parapharyngeal Space Abscess**

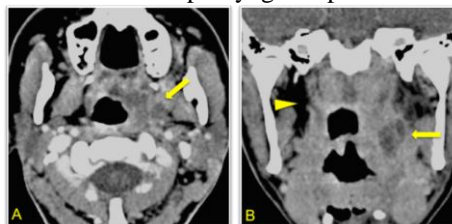


**Fig A.** Axial CECT image showing ill-defined hypodense collection in left tonsillar region (arrow), extending laterally to involve the left PPS, suggestive of lateral spread of a peritonsillar abscess. **Fig B.** Coronal reconstructed CECT image showing ill-defined hypodense collection in left PPS (arrow), causing obliteration of its fat. Compare with normal PPS on the right (arrowhead).

**MASTICATOR SPACE**

**Case 2: Adamantinoma In Left Masticator Space**

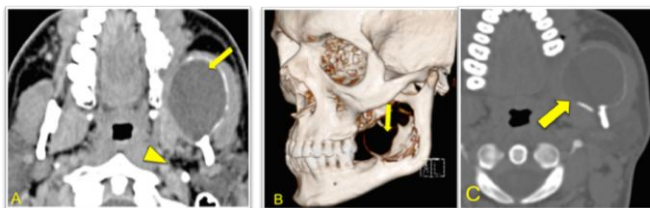


**Fig A.** Axial CECT image showing an expansile lytic lesion with peripheral rim of thinned out bone in ramus of left mandible (arrow) in the MS, displacing PPS posteriorly (arrowhead). Normal left PPS (curved arrow). **Fig B.** Volume rendered reconstruction (VRT) image and **fig (C)** Bone window CT image, demonstrating the lesion in the mandible.

**Case 3: Inflammation In Right Masticator Space.**

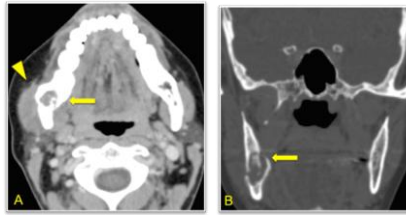


**Fig A.** Axial CECT image showing ill defined destructive lesion at the site of dental extraction in the right mandible (arrow) with bulky masseter muscle (arrowhead) and mild adjacent fat stranding. Green arrow-opposite masseter muscle. **Fig B.** Coronal reconstructed CT image in bone window setting showing destructive lesion in the mandible.

**Case 4: Ivory osteoma In Masticator space.**

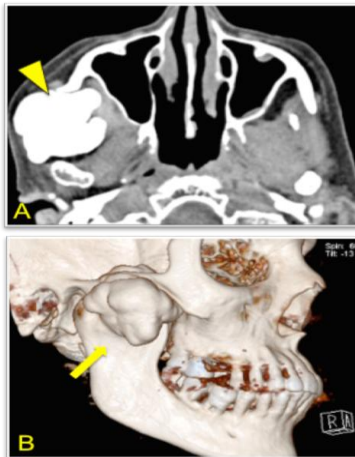


**Fig A.** Axial CT image showing large exophytic, osteogenic mass arising from neck of right mandible in the masticator space (arrowhead). **Fig B.** Volume rendered reconstruction image showing the osteogenic nature of lesion and relation to mandibular neck (arrow).

**PAROTID SPACE**

**Case 5: Right Parotid Gland Abscess.**

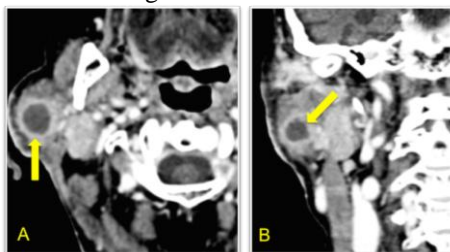


**Fig A.** Axial CECT image showing well-defined hypodense lesion in superficial lobe of right parotid gland with peripheral enhancement (arrow). **Fig B.** Coronal reconstructed image showing peripherally enhancing right parotid abscess (arrow).

**Case 6: Warthins Tumor in Right Parotid Gland.**

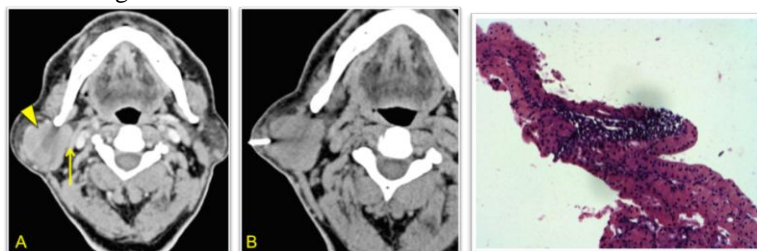


**Fig A.** Axial CECT image showing well defined homogeneously enhancing mass lesion (arrowhead) in the superficial as well as deep lobe of right parotid gland. Posterior belly of digastrics muscle is seen

separating parotid space from carotid space (arrow). **Fig B.** Axial plain CT image showing biopsy needle in-situ in right parotid gland. It was diagnosed as Warthin's tumor on histopathological examination.

**Case 7: Pleomorphic adenoma**

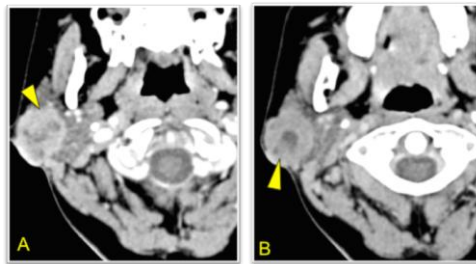


**Fig A.** Axial CECT image in venous phase showing well defined lobulated enhancing lesion with foci of hypodensities in superficial lobe of right parotid (arrowhead). **Fig B.** Axial CECT in delayed phase showing central hypodensity with peripheral enhancement.

**Case 8: Carotid body tumor.**

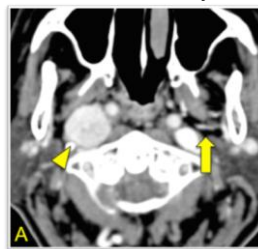


**Fig A.** Axial CECT image in arterial phase showing intensely enhancing mass lesion (arrowhead) in the carotid space, splaying the ICA and ECA, with anterior displacement of ipsilateral right PPS suggestive of carotid body tumor. Arrow indicates normal Left PPS.

**Case 9: Metastatic Lymphadenopathy in Carotid Space.**

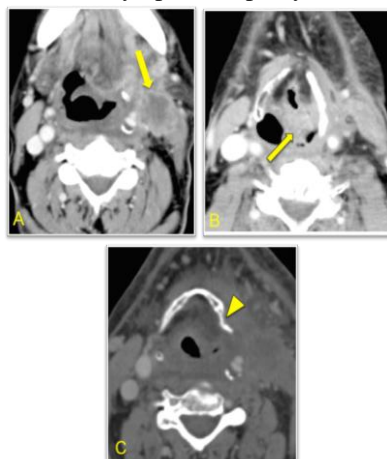


**Fig A.** Axial CECT image showing large ill defined necrotic lymphadenopathy in the left carotid space (arrow). **Fig B.** Axial CECT image showing mass involving left pyriform sinus and left aryepiglottic fold with metastatic lymphadenopathy in left of carotid space (arrow).

**Fig C.** Axial NECT image in bone window setting showing erosion of thyroid cartilage by the lesion (arrowhead).

**Case 10: Retropharyngeal abscess**

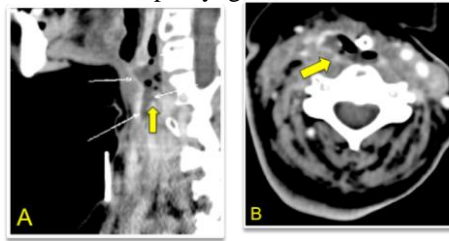


**Fig A, B** – Sagittal and axial CECT images showing ill-defined hypodense collection in the RPS containing specks of air.

**Case 11: Adenoidal hypertrophy**

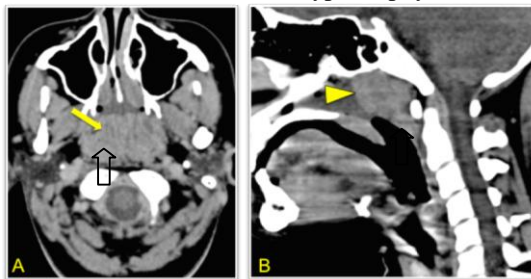


**Fig A.** Axial CT image showing enlarged adenoids indenting the airway with lateral displacement of the PPS (green arrow). **Fig B.** Sagittal CT image showing enlarged adenoids measuring 20mm (Normal = 12mm), indenting the nasopharyngeal airway.

**Case 12: Tonsillar abscess.**

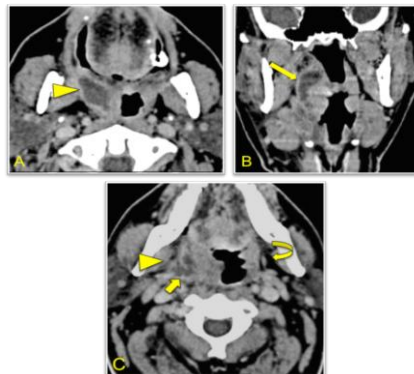


**Fig A:** Axial CECT image showing ill defined peripherally enhancing abscess in the right tonsillar and peritonsillar region (arrowhead) mildly indenting the oropharynx. **Fig B:** Coronal CECT image showing abscess extending along lateral pharyngeal wall till the level of vallecula. **Fig C:** Axial CT image showing abscess (arrow) displacing the PPS laterally (arrowhead), Normal left PPS (curved arrow).

**Case 13: Non Hodgkins Lymphoma**



**Fig A.** Axial CECT image showing homogeneously enhancing soft tissue along the tonsillar pillars causing narrowing of the oropharynx (arrow). **Fig B & C.** Similar enhancing soft tissue is noted in the posterior wall and roof of the nasopharynx (arrow) obliterating the fossa of Rosenmuller and narrowing the nasopharyngeal airway.

**Case 14: Carcinoma soft palate**

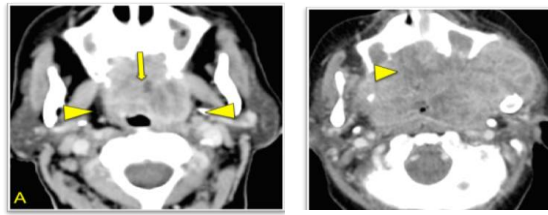


**Fig A.** Axial CECT image showing ill defined heterogeneously enhancing lesion in pharyngeal mucosal space arising from soft palate (arrow), displacing PPS laterally (arrowhead). **Fig B.** Axial CECT image of same patient after 4 month follow up shows considerable enlargement of the mass lesion with extension to masticator space (arrow) and PPS, destruction of left ramus of mandible and significant narrowing of oropharyngeal airway.

**PERIVERTEBRAL SPACE**

**Case 15: Koch's spine**

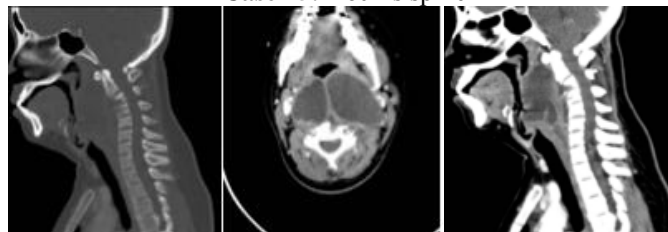


**Figure A.** Sagittal CT scan image with contrast showing the big abscess extending to the level of posterior aspect of superior mediastinum with narrowing of supraglottic area. There is marked erosion of C2 and C3 vertebra. **Figure B.** Axial CT scan image showing the prevertebral collection (retropharyngeal and parapharyngeal) at level of C3. Carotid vessels displace laterally. **Figure C.** Lateral CT scan image with out contrast showing the big abscess. There is marked erosion and rarefactions of C2 and C3 vertebra.

**POSTERIOR CERVICAL SPACE**

**Case 16: Lymphoma.**

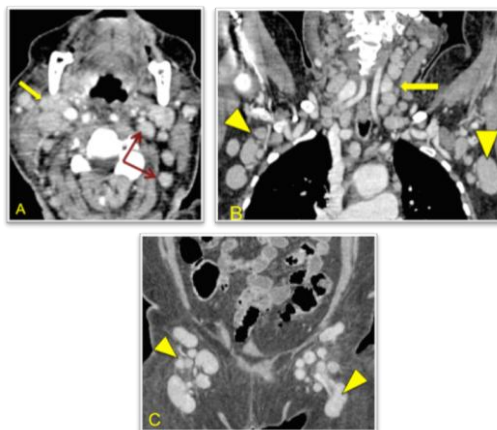


**Fig A,B,C:** CECT images showing multiple homogeneously enhancing non necrotic lymph nodes in posterior cervical space (red arrow), right carotid space (arrow). **Fig B:** Bilateral axillary (arrowheads). **Fig C:** bilateral inguinal lymph nodes (arrowheads).

**Case 17: Tuberculous lymphadenitis.**

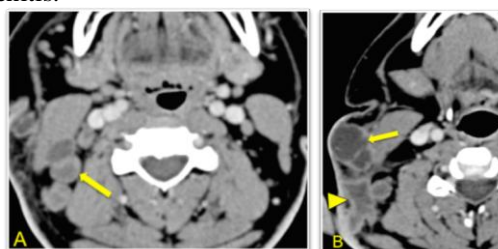


**Fig A.** Axial CECT image showing multiple necrotic peripherally enhancing lymph nodes in right posterior

cervical space (arrow). **Fig B.** Axial CECT image showing ill defined peripherally enhancing abscess (arrowhead) adjacent to necrotic lymph nodes.

**VISCERAL SPACE**

**Case 18: Parathyroid adenoma**



**Fig A & B.** Axial and sagittal reformatted CECT images in arterial phase show an oval well defined homogeneously enhancing lesion (arrowhead) in visceral space posterior to upper pole of right lobe of thyroid gland (arrow).

**Case 19: Thyroglossal Cyst**

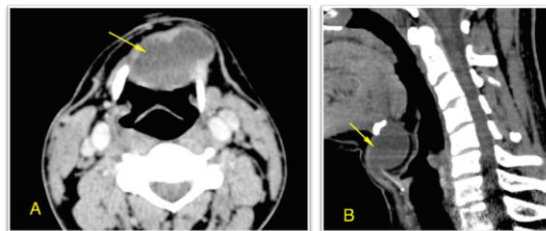


**Fig A & B:** Axial CECT and sagittal reformatted images show well-defined cystic lesion in midline in the visceral space, inferior to hyoid bone (arrows).

**Case 20: Carcinoma of Right Piriform Fossa**

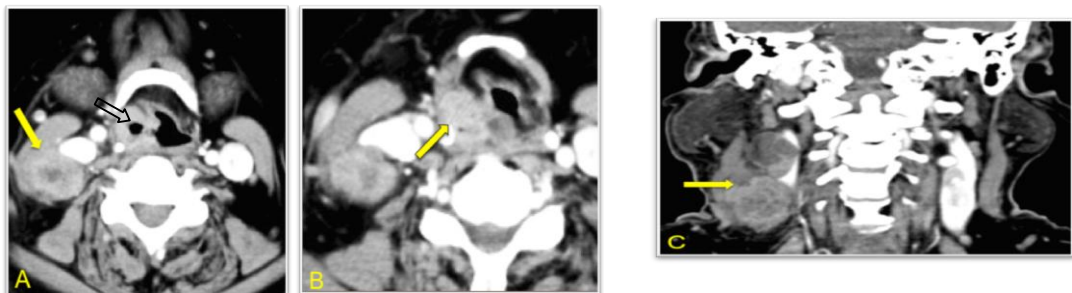


**Fig A & B:** Axial CECT image showing enhancing lesion in right piriform fossa (transparent arrow) in visceral space with metastatic lymphadenopathy at level II. **Fig C:** Coronal reformatted CECT image showing necrotic metastatic right cervical lymphadenopathy (yellow arrow).

**Case 21: Carcinoma of Epiglottis**

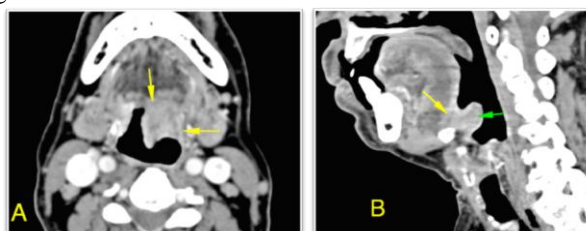


**Fig A.** Axial CECT image showing lesion in visceral space arising from epiglottis (arrow). **Fig B.** Coronal reconstructed CT image showing epiglottic lesion (green arrow) extending to and obliterating the air filled vallecula (yellow arrow).

**Case 22: Carcinoma of Thyroid Gland.**

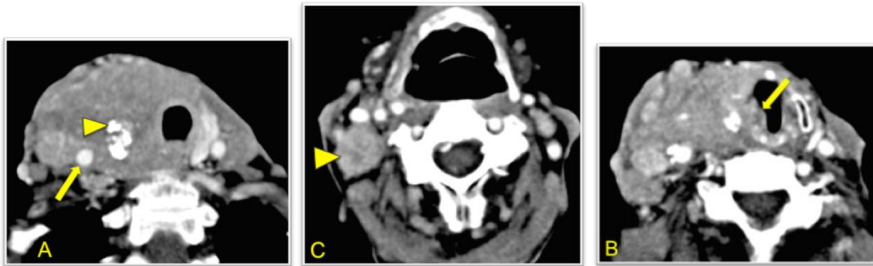


**Fig A.** Axial CECT image showing a large heterogeneously enhancing ill defined mass lesion in the visceral space arising from right lobe of thyroid, extending posteriorly into the retropharyngeal space, with focal areas of calcification (arrowhead) and vascular encasement (arrow).

**Fig B.** Axial CECT image showing infiltration of lesion into right vocal cord (arrow).

**Fig C.** Axial CECT image showing large necrotic metastatic cervical lymphadenopathy (arrowhead) on right side, in carotid space.

**Case 23 : Post Cricoid Carcinoma**

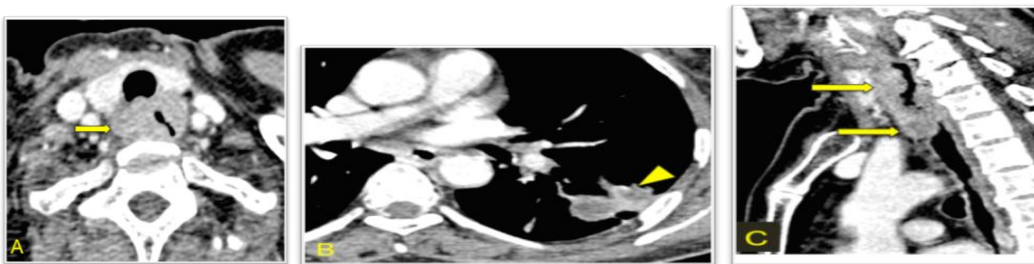


**Fig A & C:** Axial and sagittal CECT images showing circumferential enhancing mass lesion arising from post-cricoid esophagus, extending from the level of C3 to C5 vertebral bodies.

**Fig B.** Axial CECT image of lung showing evidence of necrotic metastases involving left lung.

**SUBMANDIBULAR SPACE.**

**Case 24: Acute on chronic Sialadenitis**

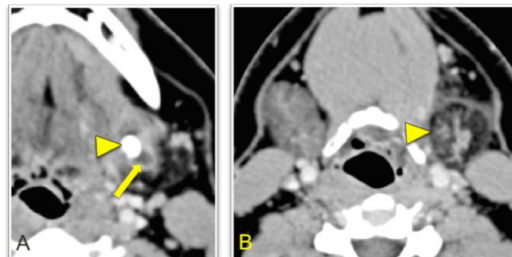


**Fig A.** Axial CECT image showing a large calculus in the left submandibular gland (arrowhead), with a peripherally enhancing abscess (arrow) adjacent to the calculus. **Fig B.** Axial CECT image showing fatty infiltration and atrophy of left submandibular gland reflecting changing of chronic sialadenitis (arrowhead) with normal gland on right.

**Case 25: Submandibular Abscess**

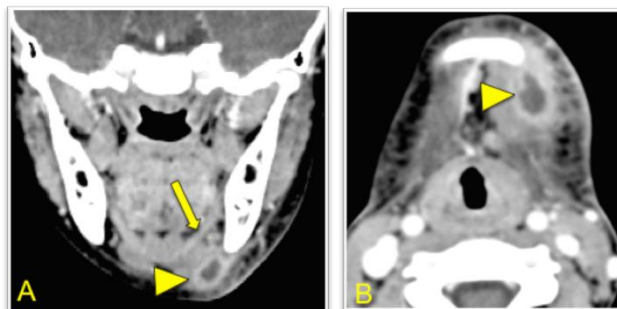


**Fig A & B.** Coronal CECT image showing ill defined, hypodense collection inferior to mylohyoid muscle

(arrow) in the submandibular space with peripheral enhancement and surrounding fat stranding (arrowhead) suggestive of abscess.

**SUBLINGUAL SPACE.**

**Case 26: Plunging Ranula.**

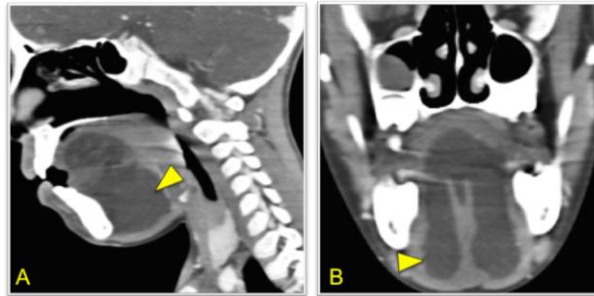


**Fig A & B:** Sagittal and coronal reformatted CT images show cystic lesion in sublingual space with inferior extension into the submandibular space suggestive of a plunging ranula.

**Case 27: Buccal carcinoma with extension into buccal space**



**Fig A.** Axial CECT image showing large ill defined heterogeneously enhancing mass lesion (yellow arrow) in right buccal space, infiltrating the right masseter muscle (transparent arrow).

**Fig B.** Normal fat filled buccal space on left side (yellow arrow).

**Fig C:** Coronal reformatted CECT image reveals right-sided level II necrotic metastatic lymphadenopathy.

**V. Conclusion**

MDCT proved to be a very useful non-invasive tool in accurately diagnosing and characterizing neck lesions with respect to neck space. The faster scan acquisition, reduced artifacts from patient motion, lower cost, are its advantages. Multiplanar reconstruction improves the localization and extent of neck lesions. It is useful for diagnosis, management and follow up of benign and malignant conditions of neck.

**References**

- [1]. Alberico RA, Husain SH, Sirotkin I. Imaging in head and neck oncology. *Surg Oncol Clin N Am.* 2004 Jan;13(1):13-35.
- [2]. Pushpender G, Satish KB, Gopesh M, Vineeta R. Role of Multislice Spiral CT in the Evaluation of Neck Masses. *JIMSA* 2013;26(1):51-4.
- [3]. Wippold FJ. 2nd, Head and Neck Imaging: The Role of CT and MRI. *J Magn Reson Imaging* 2007;25(3):453-65.
- [4]. Ozkiris M, Kala M. Histopathological examination of patients operated on for a neck mass:4-year follow-up results. *Turkish J of pathol* 2011;27(2):1347.
- [5]. Abhinandan B , Chakraborty A, Purkaystha P. Prevalence of head and neck cancers in the north east - an institutional study. *Indian Journal of Otolaryngology and Head and Neck Surgery* 2006;58(1).
- [6]. Lasrado S, Prabhu P, Kakria A, Kanchan T, Pant S, Sathian B. Clinico-pathological Profile of Head and Neck Cancers in the Western Development Region, Nepal: A 4-Year Snapshot. *Asian Pacific Journal of Cancer Prevention*,2012; 12.
- [7]. Maurea S, Cuocolo A, Reynolds JC, Neumann RD, Salvatore M. Diagnostic imaging in patients with paragangliomas - Computed tomography, magnetic resonance and MIBG scintigraphy comparison. *Q J Nucl Med.* 1996;40(4):365-71.
- [8]. Kurabayashi T, Ida M, Yoshino N, et al. Computed tomography in the diagnosis of buccal space masses. *Dento maxillofac Radiol.* 1997;26(6):347-53.
- [9]. Kimura Y, Sumi M, Sumi T, Yoshiko A, Eiichiro A, Takashi N. Deep extension from carcinoma arising from the gingiva: CT and MR imaging features. *AJNR Am J Neuroradiol* 2002;23:468-72.
- [10]. Zoumalan RA, Kleinberger AJ, Morris LG, Ranade A, Yee H, DeLacure MD. Lymph node central necrosis on computed tomography as predictor of extracapsular spread in metastatic head and neck squamous cell carcinoma: pilot study. *J Laryngol Otol.* 2010;124(12):1284-8.

- [11]. Ghosh B, Saha S, Chandra S, Nandi TK, Bera SP. Juvenile nasopharyngeal angiofibroma-three years experience. *Indian J Otolaryngol Head Neck Surg.* 2003;55(4):228–33.
- [12]. Federici S, Silva C, Maréchal C, Laporte E, Sévely A, Grouteau E, Claudet I. Retro and parapharyngeal infections: standardization of their management. *Arch Pediatr.* 2009;16(9):1225-32.
- [13]. Geoffrey DP, Harnsberger H. Radiologic Evaluation of the Normal and Diseased Posterior Cervical Space. *AJR* 1991;157(1):161-5.
- [14]. Randall GJ, Zald PB, Cohen JI, Hamilton BE. Contrast-enhanced MDCT characteristics of parathyroid adenomas. *AJR* 2009;193:538.
- [15]. Lucy YC, Fan WJ, Shen JX, Xiao P, Ai Zheng. CT features of parotid tumors: an analysis of 133 cases. *Chinese Journal of Cancer* 2007;26(11):1263-67.
- [16]. Khaled AN, Alsaid L. Deep Neck Spaces radiology and review of deep neck infections at King Abdul Aziz University Hospital. *Egyptian Journal of ear, nose, throat and Allied Science* 2010;11:110-27.
- [17].oucher C, Dorion D, Fisch C. Retropharyngeal abscesses: a clinical and radiologic correlation. *J Otolaryngol.* 1999;28(3):134-7.
- [18]. Som PM, Brandwein-Gensler MS. Chapter 40 Anatomy and pathology of the salivary gland. In: Som P, Curtin H, editors. *Head and neck Imaging.* 5th edition. Mosby-Elsevier; 2011. p. 2449–609.